Long Duration Wear Test of the NASA HERMeS Hall Thruster

Jason D. Frieman[1], Hani Kamhawi[2], George Williams[3], and Daniel Herman[4]
NASA Glenn Research Center, Cleveland, OH, USA 44135

Peter Y. Peterson[5]
Vantage Partners, LLC
NASA Glenn Research Center, Cleveland, OH, USA 44135

James Gilland[6]
Ohio Aerospace Institute
NASA Glenn Research Center, Cleveland, OH, USA 44135

and

Richard Hofer[7],
Jet Propulsion Laboratory, California Institute of Technology, Pasadena, CA, USA 91109

The NASA Hall Effect Rocket with Magnetic Shielding (HERMeS) 12.5-kW Hall thruster is the subject of extensive technology maturation by NASA GRC and JPL in preparation for development into a flight propulsion system. As part of this on-going effort, a series of three wear tests have been conducted to identify erosion phenomena and the accompanying failure modes as well as to validate service-life models for magnetically-shielded thrusters. This paper presents an overview and summary of the results obtained over the first 1715 h of the third wear test, which has the overall goal of serving as a pathfinder to identify and correct design or facility issues prior to the flight qualification campaign. Overall, negligible changes in performance and stability are observed as a function of operating time as well as relative to previous wear tests. Erosion of the inner and outer front pole covers is shown to vary by 76-300% as a function of discharge voltage and by up to 40% as a function of magnetic field strength. Shifting the cathode position upstream relative to the pole covers is shown to reduce keeper erosion rates by 84%, which supports this approach for mitigating the elevated keeper wear observed during previous wear tests.

I.Introduction

NASA continues to evolve a human exploration approach for beyond low-Earth orbit and seeks to do so, where practical, in a manner involving international, academic, and industry partners [1]. Towards that end, NASA

[1] Research Engineer, Electric Propulsion Systems Branch, jason.d.frieman@nasa.gov, Member AIAA
[2] Senior Research Engineer, Electric Propulsion Systems Branch, hani.kamhawi-1@nasa.gov, Associate Fellow AIAA
[3] Research Engineer, Electric Propulsion Systems Branch, george.j.williams@nasa.gov, Associate Fellow AIAA
[4] Research Engineer, Electric Propulsion Systems Branch, daniel.a.herman@nasa.gov, Associate Fellow AIAA
[5] Senior Research Engineer, Electric Propulsion Systems Branch, peter.y.peterson@nasa.gov, Associate Fellow AIAA
[6] Research Team Manager, Electric Propulsion Systems Branch, james.h.gilland@nasa.gov, Associate Fellow AIAA
[7] Senior Engineer, Electric Propulsion Group, richard.r.hofer@ nasa.gov, Associate Fellow AIAA

publicly presented a reference exploration concept at the Human Exploration and Operations Mission Directorate (HEOMD) Committee of the NASA Advisory Council meeting on March 28, 2017 [2]. This approach is based on an evolutionary human exploration architecture, expanding into the solar system with cis-lunar flight testing and validation of exploration capabilities before crewed missions beyond the Earth-Moon system and eventual crewed Mars missions.

High-power solar electric propulsion is one of those key technologies that has been prioritized because of its significant exploration benefits. Specifically, for missions beyond low Earth orbit, spacecraft size and mass can be dominated by onboard chemical propulsion systems and propellants that may constitute more than 50 percent of the spacecraft mass. This impact can be substantially reduced through the utilization of Solar Electric Propulsion (SEP) due to its substantially higher specific impulse. Studies performed for NASA's HEOMD and Science Mission Directorate have demonstrated that a 40-kW-class SEP capability can be enabling for both near term and future architectures and science missions [3]. In addition, a high-power, 40 kW-class Hall thruster propulsion system provides significant capability and represents, along with flexible blanket solar array technology, a readily scalable technology with a clear path to much higher power systems.

Accordingly since 2012, NASA has been developing a Hall thruster electric propulsion string that can serve as the building block for realizing a 40-kW-class SEP capability. The Hall effect thruster (HET) system development, led by the NASA Glenn Research Center (GRC) and the Jet Propulsion Laboratory (JPL), began with maturation of the NASA Hall Effect Rocket with Magnet Shielding (HERMeS) and power processing unit. The technology development work has transitioned to Aerojet Rocketdyne via a competitive procurement selection for the Advanced Electric Propulsion System (AEPS) contract. The AEPS contract includes the development, qualification, and delivery of multiple flight electric propulsion strings. The AEPS Electric Propulsion (EP) string consists of the Hall thruster, power processing unit (including digital control and interface functionality), xenon flow controller, and associated intra-string harnesses. NASA continues to support the AEPS development by leveraging in-house expertise, plasma modeling capability, and world-class test facilities. NASA also executes AEPS and mission risk reduction activities to support the AEPS development and mission application.

As part of this effort, NASA has completed two wear tests to identify erosion phenomena and the accompanying failure modes as well as to validate service-life models for magnetically-shielded thrusters. These tests utilized two different technology demonstration unit (TDU) thrusters with similar designs, but different cathode configurations. The first began in 2016 and accumulated approximately 1700 hours of operation using the TDU-1 thruster at the nominal operating condition (600 V, 12.50 kW) [4]. In this test, the cathode keeper was positioned upstream of the inner front pole cover, and negligible keeper erosion was observed [4, 5].

The second wear test was performed in 2017 with the TDU-3 thruster and is referred to as the TDU-3 Short Duration Wear Test (SDWT) [5]. Instead of one long segment, the SDWT was divided into a series of seven short duration segments each lasting for approximately 200 hours at a different thruster operating condition [5]. For all of these segments, the keeper was coplanar with the downstream surface of the inner front pole cover, which represents a downstream shift relative to the TDU-1 position by a distance approximately equal to the thickness of the inner front pole cover [5]. Despite this small shift, results from the SDWT indicated average keeper erosion rates of approximately 80 μm/kh at the same operating condition used for the TDU-1 wear test, which were the largest rate observed for any thruster component during the SDWT [5]. Taken together with the results from the TDU-1 wear test, these measurements suggest that the axial position of the cathode can impact keeper erosion rates and, in part, motivate the need for a third wear test in order to identify and characterize such sensitivities.

This work presents an overview and summary of the results obtained to date from the third wear test (named the TDU-3 Long Duration Wear Test or TDU-3 LDWT), which began in October 2017. This test has three overall goals. The first is to provide additional insight into thruster performance, stability, plume, and wear trends over extended periods of operation in order to identify any potential issues that can be corrected in the final AEPS HET design. Towards that end, the cathode was returned to the position used during the TDU-1 wear test (i.e., upstream of the inner front pole cover), but the keeper thickness was doubled in order to investigate this as an approach for mitigating the elevated keeper wear observe during the SDWT [5].

The second goal of the TDU-3 LDWT is to further quantify the impact of facility backsputter on thruster operation in order to determine if any further design refinements are required to limit AEPS hardware sensitivity to extended operation during ground testing. Finally, this test is designed to serve as a pathfinder for the planned life and qualification testing of the hardware to be delivered as part of the AEPS contract as well as two novel diagnostics intended for use as part of the qualification campaign: a thrust vector probe and in-situ wear tool. Thus, the TDU-3 LDWT provides NASA the opportunity to develop the experience and procedures for operating high-power long duration tests, as well as additional insight into the factors that influence component lifetime.

II.Experimental Apparatus

A. HERMeS TDU-3

All experiments detailed in this work were performed using the 12.5-kW NASA HERMeS TDU-3. The overall HERMeS design incorporates technologies developed by NASA over nearly two decades, including a magnetic shielding topology to eliminate discharge channel erosion as a life-limiting mechanism. The result is a significant increase in the operational lifetime of state-of-the-art HETs, with HERMeS being designed to operate at a specific impulse of 3000 s for an operational lifetime exceeding 50 kh [6–10].

The HERMeS TDU-3 thruster is shown in the configuration used for the LDWT in Fig. 1. As discussed in the introduction, the thruster configuration is largely unchanged from that used during the SDWT, with the exception of the thickness and position of the cathode keeper [5]. In addition, a pair of new magnet coils were installed in TDU-3 prior to the LDWT. This resulted in a change in the current settings required to achieve a fixed magnetic field strength, but did not change the magnetic field shape. Although the cathode position used during the LDWT matches that used during the TDU-1 wear test, a number of other small design changes differentiate TDU-3 and TDU-1 including a change in the grade of boron nitride used for the discharge channel. A detailed description of these changes is provided in Kamhawi et al. [7]; the results from that work suggest they result in minimal changes to HET performance, stability, and plume properties.

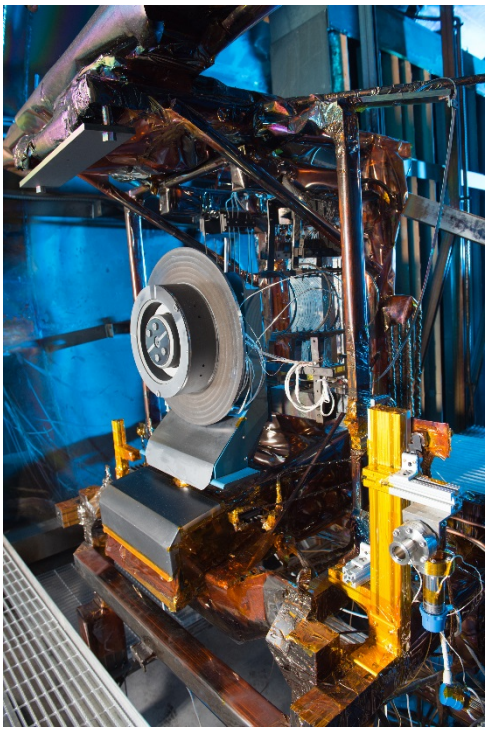

Fig. 1 HERMeS TDU-3 Hall thruster in the configuration used for the LDWT.

Xenon propellant was supplied to the thruster and the centrally-mounted cathode using a laboratory feed system composed of stainless-steel lines metered with commercial thermal mass flow controllers. The anode line was metered using a 500-sccm controller, and the cathode line was metered using a 100-sccm controller. All controllers were calibrated before and after the test using a NIST-traceable, positive displacement primary piston prover and have an uncertainty approximately 1% of the measurement [11].

All power to TDU-3 was provided using a power console composed of commercial laboratory power supplies. The discharge was controlled using three 15-kW (1000 V, 15 A) power supplies connected in a master-slave configuration. The output from these supplies was connected to a laboratory wire harness with an inductance and capacitance of approximately 2.5 μH and 236 pF, respectively [12]. This console is equipped with a set of safety interlocks that allows the data acquisition or vacuum facility control system to disable power and place the thruster in a safe state in the event that a facility or thruster anomaly is detected. This setup is unchanged from previous HERMeS characterization and wear tests [4, 5, 7, 13–15].

Following the results from the electrical configuration study performed by Peterson et al. [15], the TDU-3 thruster body was electrically tied to the cathode, and all conductive surfaces within approximately one meter of the thruster exit plane were insulated using dielectric sheeting [15, 16]. This was done in order to provide better control over the number of electrical coupling paths between the HET and facility in the near-field [15, 16].

Thruster telemetry was recorded continuously at a rate of 1 Hz using a multiplexed data acquisition system. End-to-end calibrations of the laboratory power and data acquisition systems (DAQ) were performed before and after the test using a NIST-traceable digital multimeter. The resultant uncertainty was approximately ±0.06 V and ±0.03 A for measurements of voltage and current, respectively. Discharge current oscillations were measured using a 150-A AC/DC current probe connected to an oscilloscope; oscillations in discharge voltage and cathode-to-ground voltage were measured continuously using high-voltage differential probes connected to the same oscilloscope. All oscillation data were sampled at a rate of 1 MS/s. The root-mean-square (RMS) and peak-to-peak values were computed by the oscilloscope over intervals composed of 100,000 samples and recorded by the data acquisition system.

B. Vacuum Facility

All experiments detailed in this work were performed in Vacuum Facility 5 (VF-5) at NASA GRC. VF-5 is a cylindrical chamber measuring 4.6 m in diameter and 18.3 m in length [17]. For this test, VF-5 was evacuated using

a series of cryopumps. The cryopumps have a total effective pumping area of 33.5 m^2 and a combined nominal pumping speed of approximately 700,000 l/s on xenon [17–19]. In order to obtain the lowest possible background pressure, the thruster was installed in the main volume of VF-5 at the same location previously used during the TDU-1 wear test and the TDU-3 SDWT [4, 5]. The placement of the cryopumps relative to the thruster at this location as well as the resultant near-field background neutral distribution is described in previous work [17–19].

Facility pressure was monitored with two xenon-calibrated, Bayard-Alpert style hot-cathode ionization gauges. The first (IG#2) has a downstream-facing orifice and was mounted on a boom arm at a location approximately 0.8 m radially outward from the centerline of the thruster. The second (IG#3) was located approximately 0.7 m radially outward and centered approximately 0.08 m upstream of the HET exit plane. The orifice of IG#3 faced radially outward (i.e., away from the HET). Both gauges were configured for operation with electric propulsion systems and thus had an elbow and plasma screen installed on the inlet of the gauge [20]. The housing of each was also attached to facility ground via an electrical grounding strap to avoid charging effects. A thermocouple was installed on the exterior of each ion gauge tube, thus allowing the measured pressures to be corrected for thermal effects [21]. The gauge temperatures and pressures were sampled using the same multiplexed DAQ used to record thruster telemetry [20]. Consistent with previous tests performed in VF-5, all pressures reported in this work correspond to the measurements made using IG #3 [4, 5, 13–15].

Measurements of facility backsputter were obtained using three quartz crystal microbalances (QCMs) [22]. The QCMs were located approximately 1 meter radially outward from the centerline of the thruster in the thruster exit plane. All three QCMs faced downstream and were water cooled with three parallel cooling loops from a single chiller. The total deposited thickness was measured by the QCM controller and recorded by the same DAQ used for thruster telemetry. The measured thickness was then post-processed in order to compute the average backsputter rate using the techniques described by Gilland et al [22].

C. Thrust Stand

Thrust was measured using the same null-type inverted pendulum thrust stand used in previous HERMeS performance characterization and wear tests [4, 5, 7, 13, 15, 23]. The design and theory of operation of the thrust stand are detailed in several previous works [24–26]. For this work, the thrust stand was operated in a null-coil configuration. In this configuration, the position of the thruster is measured by a linear variable differential transformer (LVDT) and maintained by a pair of electromagnetic actuators. The current through each actuator is controlled using an integral-differential controller that use the LVDT signal as the input and then modulate the current through the actuators in order to hold the thruster stationary. The thrust is then correlated to the resultant current through the actuators. The thrust stand is also equipped with a closed-loop inclination control circuit, which uses an integral controller and piezoelectric actuator to maintain the inclination measured by an electrolytic tilt sensor and thus minimize thermal drift during performance measurements. The thrust stand was calibrated before and after each performance characterization period by loading and offloading a set of known weights using an in-situ pulley system. The thrust stand uncertainty for this work is approximately 0.8% of the measurement [27].

D. Wear Measurements

All erosion measurements were made with a chromatic, white-light non-contact benchtop profilometer. The employed profilometer is equipped with an optical pen oriented normal to the HET exit plane with a 3-mm measuring range. All acquired profilometry data were analyzed according to the guidance established in the ISO 5436-1 measurement standard for a type A1 step (i.e., a wide groove with a flat bottom) [28]. A detailed uncertainty quantification was performed for each data point analyzed using the ISO method that accounts for instrument error, surface roughness, wear due to operation at points other than the nominal wear point, and the non-flat nature of the acquired profiles. The results of this uncertainty analysis yielded typical uncertainties on the order of ±2 μm for this work.

Data acquired near the mask fasteners were not able to be analyzed using the aforementioned ISO method due to the interruption of the unexposed reference surface by the hole for the fastener. This resulted in a step width that was insufficient for this analysis technique. Data in this region were analyzed manually using commercial software provided by the profilometer manufacturer. This manual technique is identical to that used during previous wear tests and generates results that differ from those of the ISO technique by less than the measurement uncertainty. However, for clarity, data analyzed using the manual method are shown without error bars. It is important to note that all presented wear rates are computed as the total measured step height divided by the total operating time for that component, and therefore represent the average erosion rate over the stated interval.

III.Results and Discussion

A. Test Segment Overview

All results presented in this work were acquired during the first four segments of the TDU-3 LDWT. Segment I was performed at the nominal TDU operating condition of 600 V, 12.5 kW and resulted in the accumulation of 1015 h of operating time. It is important to note that this segment was interrupted by a facility anomaly and so was completed in two consecutive parts lasting 620 h and 395 h, respectively. Segments II-IV were all performed at the 300 V, 6.25 kW throttle point, however, each was performed at a different magnetic field strength. Segment II was performed at the nominal magnetic field strength while Segments III and IV were performed at 75% and 125% of the nominal strength, respectively. Each of these segments lasted for between 200 and 250 hours. A summary of these segments is shown Table 1. Since all wear conditions used the same discharge current (20.83 A), throughout this work, wear conditions will be specified using the syntax xxx V/yyy B where xxx represents the discharge voltage and yyy is the fraction of nominal magnetic field strength.

Similar to the approach taken in previous TDU wear tests, continuous operation at each of the conditions listed in Table 1 was periodically interrupted in order to acquire performance and stability data for the reference firing conditions shown in Table 2. Average facility pressure was approximately 3 μTorr-Xe for operation at RFC 1 and 4.5 μTorr-Xe for all other conditions. Overall, these characterizations resulted in the accumulation of approximately 3% of the total operating time at throttle conditions other than the specified wear point.

Table 1 Summary of completed TDU-3 LDWT test segments.

Segment		I	II	III	IV
Operating Condition		600 V/1 B	300 V/1 B	300 V/0.75 B	300 V/1.25 B
Operating Time (h)		1015*	248	213	239
Performance Characterization Intervals (h)		0, 250, 500, 620,1000	115, 248	0, 71, 213	0, 239
Wear Characterization Intervals (h)		620, 1000	248	213	239
IFPC Configuration	*New*	Yes	Yes	Yes	Yes
	Material	Polished Graphite	Polished Graphite	Polished Graphite	Polished Graphite
	Mask Locations†	2 and 8	2 and 8	2 and 8	2 and 8
OFPC Configuration	*New*	Yes	No	No	Yes
	Material	Polished Graphite	Polished Graphite	Polished Graphite	Polished Graphite
	Mask Locations†	12 and 9	8	4	12 and 9
Keeper Configuration	*New*	Yes	No	No	No
	Material	Polished Graphite	Polished Graphite	Polished Graphite	Polished Graphite
	Tab Location†	11	-	-	11:30

*Completed in two parts: 0-620 hours, 620–1000 hours.

†Mask locations listed using equivalent clock position with 12 o'clock corresponding to the top of TDU-3. For thruster components used in previous segments, a position is listed only if an additional mask was added or the original mask was modified.

Table 2. Reference firing conditions used during the TDU-3 LDWT.

RFC	Discharge Voltage (V)	Discharge Current (A)	Discharge Power (W)
1	300	9.00	2700
2	300	20.83	6250
3	400	20.83	8333
4	500	20.83	10417
5	600	20.83	12500
6	630	20.83	13123

B. Performance and Stability Results

The performance of TDU-3 measured at each of the RFCs from Table 2 is shown as a function of total operating time in Fig. 2. It is important to note that an anomaly occurred with the inverted pendulum thrust stand during Segment III, which precluded obtaining accurate thrust measurements for the performance characterizations performed during that segment. Due to this issue, the resultant data are omitted from Fig. 2.

As shown in Fig. 2, the measured thrust of TDU-3 varied by less than the thrust stand uncertainty for all RFCs throughout the completed segments. Furthermore, the variation between the measurements obtained during the LDWT and those acquired during the SDWT and TDU-1 wear tests are also less than the measurement uncertainty [4, 5]. This performance invariance is an indicator of the effectiveness of the HERMeS magnetic shielding topology as previous wear tests performed on non-magnetically shielded thrusters have observed a decrease in performance during the first approximately 1000 h of operation [29]. The decrease in performance has been attributed to erosion of the discharge channel walls, which is a phenomenon that is minimized by magnetic shielding [29].

The stability of TDU-3 was assessed using the ratio of the peak-to-peak of the discharge current (I_{dPk2Pk}) to the average discharge current (I_d). The results are plotted alongside the thrust measurements for each of the RFCs in Fig. 2. Similar to the performance results, the discharge current oscillations varied by less than 4% for all RFCs over the first four segments of the LDWT. Furthermore, the measured stability characteristics are consistent with those obtained during previous TDU wear and performance characterizations [4, 5, 7, 13, 15, 23]. Taken together, the performance and stability results indicate that TDU-3 was operating nominally throughout the LDWT.

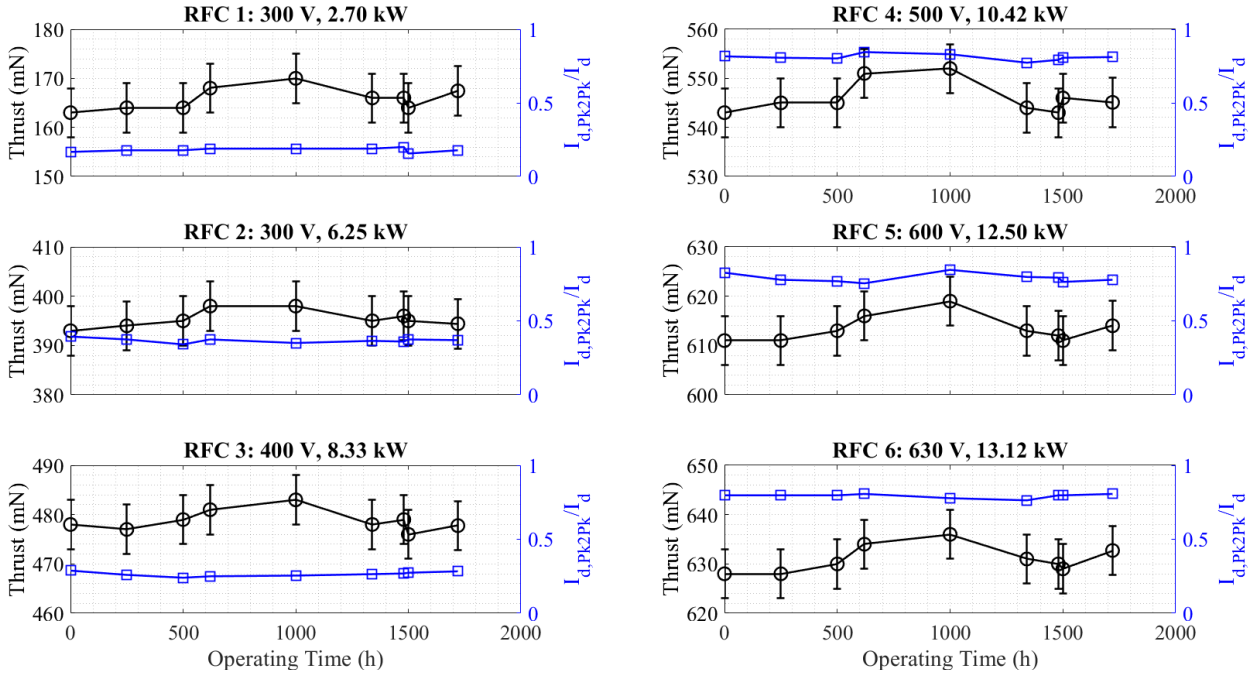

Fig. 2 Performance and stability of TDU-3 during the LDWT at each of the RFCs.

C. Wear Measurements

1. *Overview*

Similar to the approach taken in previous HERMeS wear tests, the inner front pole cover (IFPC), outer front pole cover (OFPC), and keeper were modified in order to better characterize component erosion rates [4, 5]. In order to minimize the variation in pre-test surface roughness and thus provide as uniform a baseline as possible, each of these surfaces was polished prior to installation. In addition, graphite masks were installed to provide unexposed surfaces to use as a reference for post-test analysis. Two 0.5-mm thick graphite masks were installed at the 2 o'clock and 8 o'clock locations of the IFPC. These masks are shown in Fig. 3(a) and are identical (in both dimension and location) to the graphite masks used during the SDWT [5]. In addition to masks, a series of four graphite bushings and screw caps were adhered to the bolts on the inner front pole cover in order to simulate the bosses that will be present on the Engineering Design Unit (EDU) thruster. These bushings are shown mounted at the 12 o'clock, 4 o'clock, 6 o'clock,

and 10 o'clock positions on the IFPC in Fig. 3(a). It is important to note that, as shown in Table 1, a new IFPC was installed for each operating condition in order to avoid conflation of the measured wear rates.

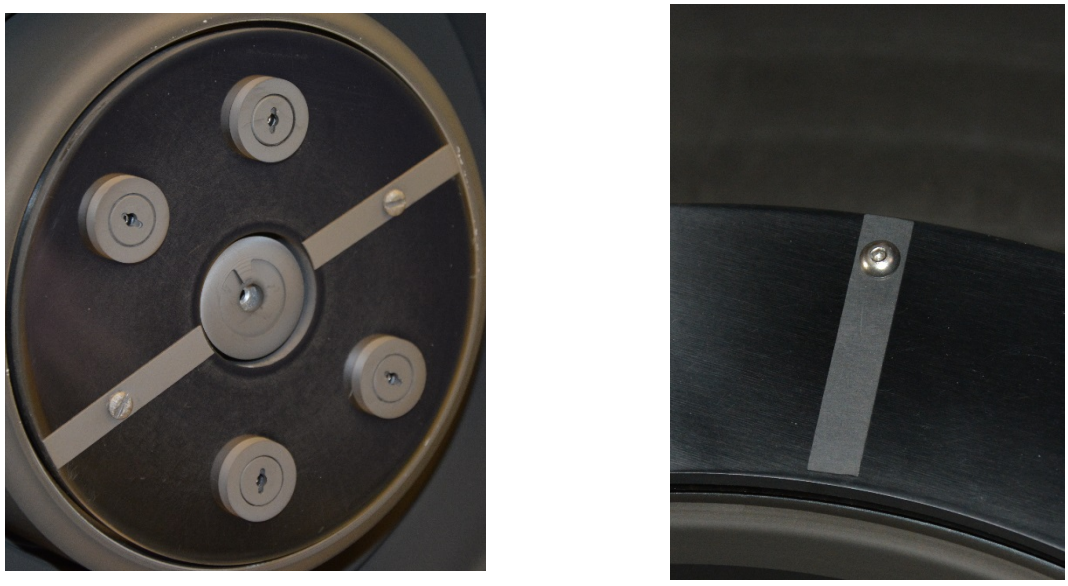

(a) **(b)**

Fig. 3 Masks and bushings installed on the TDU-3 (a) IFPC and keeper and (b) OFPC. The 12 o'clock corresponds to the top of both photos.

As shown in Fig. 3(b), a series of graphite strips were also affixed to the OFPC. These masks were identical to those used during the SDWT. Two masks were installed at the beginning of the test at the 12 o'clock and 9 o'clock positions. Unfortunately, the 9 o'clock mask rotated out of position during the first 250 h of operation, thus precluding this region from post-test analysis. Additional masks were added at the 8 o'clock and 4 o'clock positions prior to Segments II and III, respectively. A new OFPC with masks at the 12 o'clock and 9 o'clock positions was installed prior to Segment IV.

Measurements of OFPC wear were acquired after the completion of 620 h and 1000 h at the 600 V/1 B operating condition as well as after the completion of the Segments III and IV. This allows direct computation of the wear rates for each of these operating conditions. Since OFPC wear was not measured after the completion of Segment II, the OFPC erosion rate for this condition could not be directly determined and is therefore omitted from the presented results.

In order to provide a masked reference surface on the keeper, a graphite ring was affixed to the outer edge of the downstream keeper face. As shown in Fig. 3(a), a small tab was also included as part of the mask, which protruded radially inwards towards the cathode orifice. This tab enabled an assessment of the radial variation in erosion rates across the keeper face. Measurements of keeper wear were acquired after 620 h and 1000 h at the 600 V/1 B operating condition as well as after the completion of Segment IV. The keeper mask was rotated prior to the start of this last segment to expose a new region of polished graphite. This enabled direct measurements of the keeper wear for operation at 600 V/1 B and 300 V/1.25 B, as well as the average keeper erosion rate over the entire LDWT. Table 1 contains a summary of the thruster configuration and wear measurements acquired for each segment.

2. IFPC Wear

Fig. 4 shows the IFPC erosion rates measured near the 8 o'clock mask during the LDWT as a function of normalized IFPC radius. In Fig. 4, a normalized radius of 0 corresponds to the edge of the IFPC closest to the cathode whereas a radius of 1 corresponds to the edge closest to the discharge channel. It is important to note that the truncation of the data near the inner IFPC edge is due to the fact that the employed masks only cover approximately 95% of the IFPC.

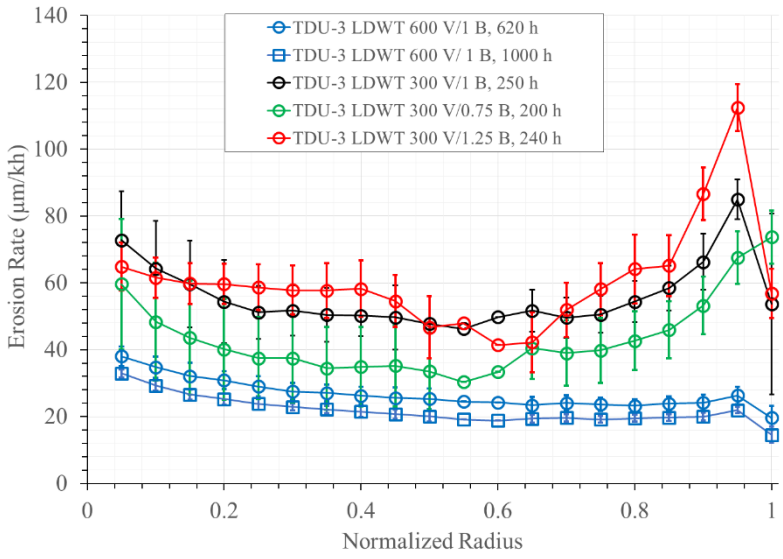

Fig. 4. IFPC erosion rates near the 8 o'clock mask from the TDU-3 LDWT.

Consistent with previous empirical and analytic results, for all operating conditions, the erosion rate is observed to minimize near the center of the IFPC and gradually increase towards the keeper and discharge channel [5, 30, 31]. It is important to note that, as shown in Fig. 5, the local maxima shown in Fig. 4 near a normalized radius of 0.9 represent a continuous trend and are, therefore, not outliers. Despite the observed consistency in radial variation, the magnitude of the erosion rate is a strong function of discharge voltage. As shown in Fig. 4, the radially-averaged erosion rate increases by approximately 76% between the 600 V and 300 V conditions performed at the nominal magnetic field strength.

As discussed in previous work, the observed erosion trends with discharge voltage are likely driven by shifts in the axial location of the acceleration region [5, 30–32]. Specifically, laser-induced florescence (LIF) measurements have shown that the acceleration region shifts downstream at lower discharge voltages [31]. This shift results in a concomitant increase in beam divergence and, thus, the number of eroding ions reaching the IFPC [5, 30, 31].

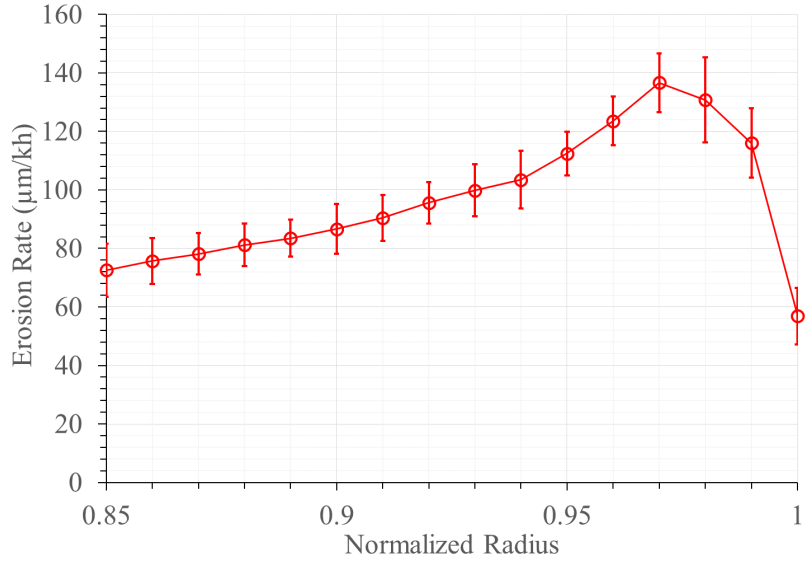

Fig. 5 IFPC erosion rates near a normalized radius of 0.9 for the 300 V/1.25 B condition.

Isolating the results from the three segments performed at 300 V provides some insight into the impact of magnetic field strength on IFPC wear. As shown in Fig. 6, erosion rates at this discharge voltage largely increased with magnetic field strength. Specifically, the radially-averaged erosion rate increased by 42% between the 0.75 B

and 1.25 B cases, which is greater than the measurement uncertainty. This increase in erosion with magnetic field strength is consistent with previous results obtained for 600 V operation [5, 31]. Although true for most radial locations, the observed increase in erosion rates with magnetic field strength does not hold in the regions near the mask fastener and IFPC edges (i.e., for normalized radii less than 0.15 and between 0.55 and 0.65). However, as discussed previously, the measurements in these regions have a much higher measurement uncertainty due to the truncation of the unexposed reference surfaces by the hole for the mask fastener. Because of this, the observed differences in wear rates in these regions are likely artifacts of these increased uncertainties and no strong conclusions can be drawn.

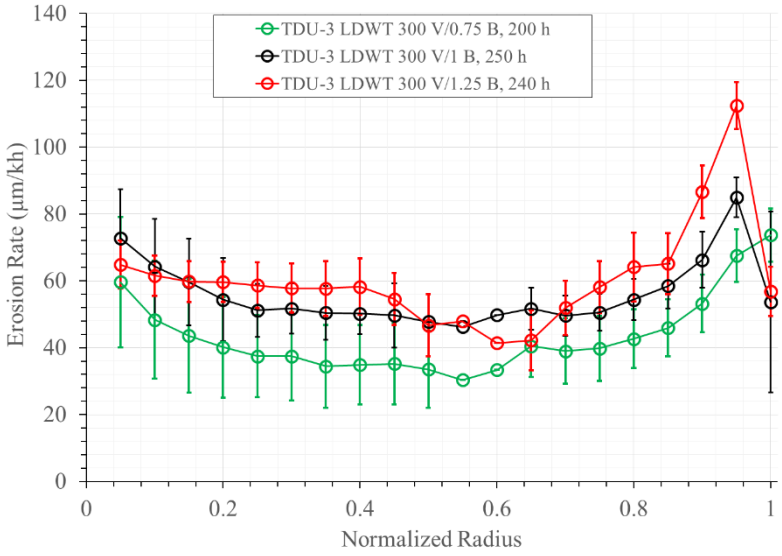

Fig. 6 IFPC erosion rates near the 8 o'clock mask for the three segments performed at 300 V.

Previous empirical studies performed for 600 V operation have shown a similar increase in IFPC erosion with increased magnetic field strength, despite the upstream shift of the acceleration zone observed at elevated magnetic fields by LIF [5, 29, 32]. Modeling results have suggested that, for discharge voltages above 500 V, the divergence of the beam is never high enough to allow eroding ions to reach the IFPC, thus nullifying the mechanism by which a downstream shift in the acceleration zone caused an increase in IFPC erosion for operation at 300 V [30]. Instead, the models have shown that the higher magnetic field strength causes a concomitant increase in sheath potential at the pole, and therefore, an increase in energy (rather than quantity) of incident ions [30]. However, these same models predict that this trend should reverse for operation at 300 V, and, therefore, that the measured erosion rates should have decreased with increased magnetic field strength due to the upstream shift in acceleration zone [30]. The cause for this discrepancy is not presently known, and, as such, further investigation may be warranted.

In addition to the impacts of discharge voltage and magnetic field on IFPC wear, the results in Fig. 4 also provide insight into how IFPC erosion changes over the thruster lifetime. Specifically, the erosion rates measured after 1000 h of operation at 600 V were lower at all radii by an average of 20% compared to those measured after 620 h of operation. This decrease in erosion rate with time is outside of the empirical uncertainty and was also observed during previous wear testing of TDU-1 [4, 5].

Similar to the approach taken in Williams et al. [4], in order to assess the azimuthal symmetry of the IFPC wear mechanism, profilometry measurements acquired near the masked regions at both 8 o'clock and 2 o'clock were compared for each operating condition. The results are shown for two operating conditions in Fig. 7. Consistent with previous results, the azimuthal variation in wear rates was less than the measurement uncertainty, suggesting that the IFPC wear process is symmetric [4]. It is important to note that although only two data sets are shown, the observed trends were consistent for all operating conditions.

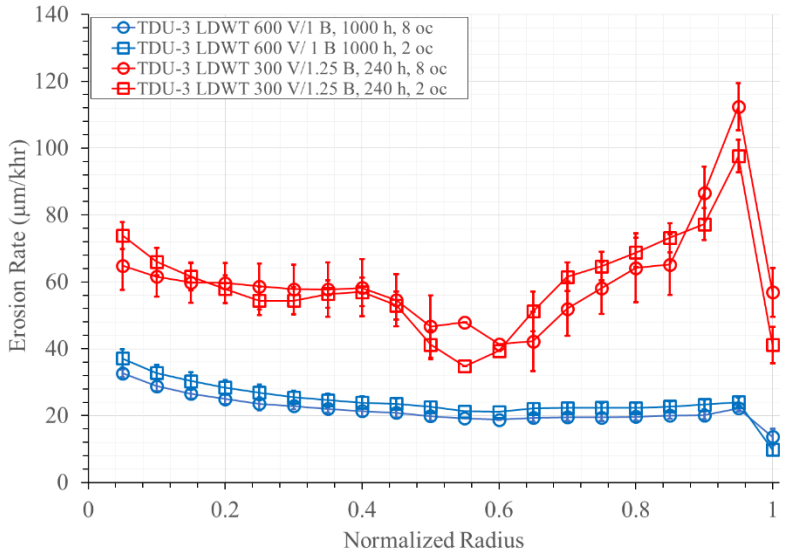

Fig. 7 Comparison of IFPC erosion rates measured near the 8 o'clock (8 oc) and 2 o'clock (2 oc) masks.

3. Keeper Wear

As stated in the introduction, one of the motivations of the LDWT was to determine if the change in cathode axial position could explain the differences in wear rates measured during the TDU-1 1700 h test and the SDWT. Towards that end, Fig. 8 shows the keeper erosion rates measured during the LDWT and SDWT as a function of keeper radius. In Fig. 8, a keeper radius fraction of 0 corresponds to the cathode orifice whereas a radius fraction of 1 corresponds to the edge closest to the IFPC. It is important to note that the truncation of the LDWT data near the outer keeper edge is due to the change in mask geometry relative to the SDWT and that the 1715 h LDWT data set corresponds to the average erosion rate over all completed test segments [5].

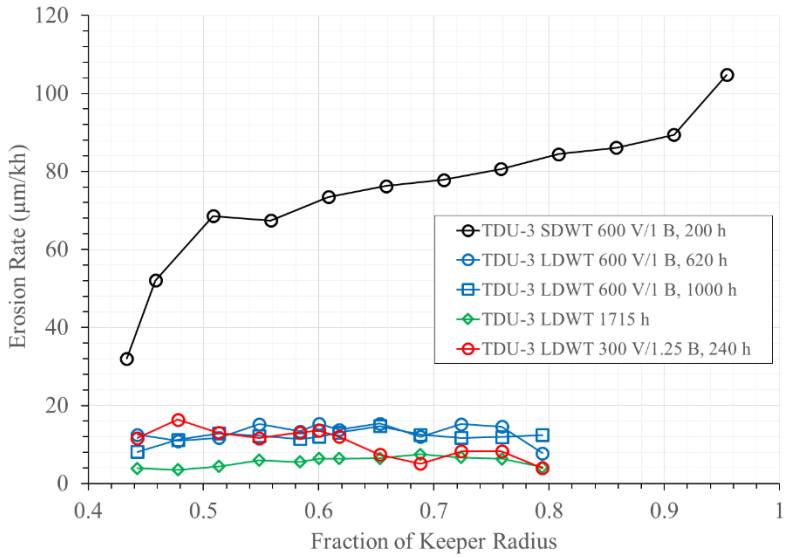

Fig. 8 Keeper erosion rates from the TDU-3 SDWT and LDWT for operation at 600 V, 12.5 kW, and nominal magnetic field

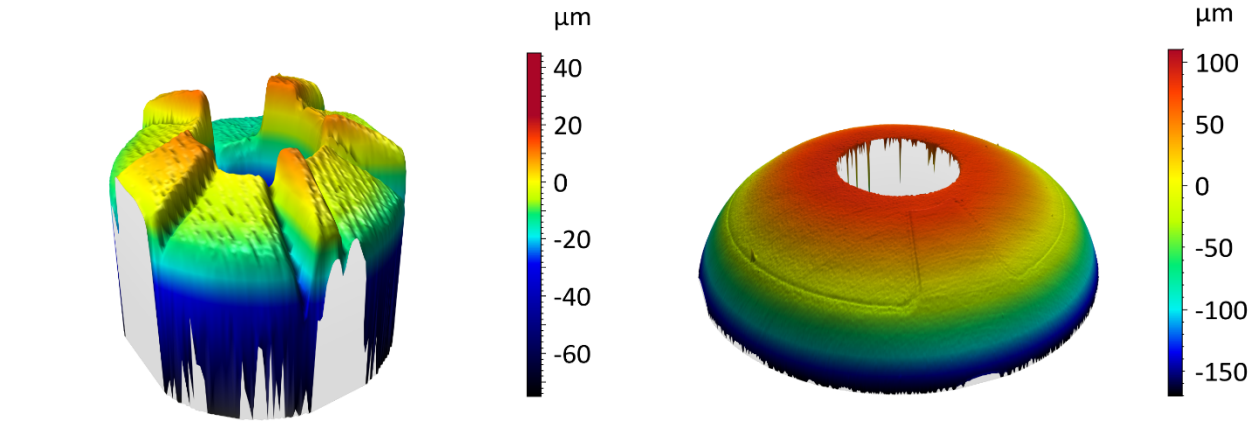

(a) **(b)**

Fig. 9 3D view of the keeper after the (a) SDWT and (b) LDWT (Segment I).

As shown in Fig. 8, the keeper during the LDWT eroded at a radially-averaged rate of approximately 13 µm/kh independent of operating condition, which represents a decrease of 84% relative to the results acquired during the portion of the SDWT operated at the 600 V/ 1 B condition [5]. Furthermore, unlike during the SDWT, no significant radial variation in erosion rate was observed [5]. Qualitative confirmation of these results is shown by features visible in the 3D renderings of the cathode keeper acquired post-test and shown in Fig. 9. Consistent with the results shown in Fig. 8, the elevated plateaus corresponding to the masked regions of the keeper are much less pronounced for the LDWT than for the SDWT. This is particularly striking as each of the unmasked regions of the SDWT keeper accumulated approximately one-fifth the hours of those on the LDWT keeper [5]. It is important to note that the surface doming observed in Fig. 9(b) was also present in pre-test scans and thus is likely an artifact of the pre-test polishing and not plasma exposure. Taken together, these results confirm the strong link between cathode position and keeper erosion rates and indicate that the upstream shift in cathode position successfully mitigated the elevated erosion rates observed during the SDWT.

It is important to note that the observed keeper step sizes were too small to be processed using the ISO method discussed previously. Instead, as done in both previous wear tests, the keeper data were analyzed manually using commercial software provided by the profilometer manufacturer. As discussed in Williams, et al. [5], the SDWT keeper erosion data at the 600 V/1 B condition was acquired during the comprehensive performance characterization of TDU-3. As such, during the SDWT, TDU-3 was operated over a range of throttle conditions and magnetic field settings, resulting in increased uncertainty in the erosion measurements [5]. However, previous work has indicated that this increased uncertainty is smaller in magnitude than the wear rate reduction observed between the SDWT and LDWT [5]. As such, the increased uncertainty associated with non-wear point operation during the SDWT does not impact the overall conclusion that the upstream shift of the cathode significantly reduced keeper erosion rates.

As discussed by Lopez Ortega, et al. [33], the decrease in keeper erosion for the upstream cathode location is likely due to an increase in shielding provided by the IFPC against ions originating close to the discharge channel. Specifically, the upstream shift reduces the effective downstream view factor of the keeper. Since it is postulated that thruster ions (i.e., those born in the thruster channel, acceleration region, or near-field plume) are the primary cause of IFPC and keeper erosion, this reduction in view factor should reduce the number of thruster ions incident on the keeper, resulting in the observed reduction in keeper erosion rates [30, 33].

4. OFPC Wear

Fig. 10 shows the OFPC erosion rates measured during the LDWT as a function of normalized OFPC radius. In Fig. 10, a normalized radius of 0 corresponds to the edge of the OFPC closest to the discharge channel whereas a radius of 1 corresponds to the outer edge of the thruster. It is important to note that the truncation of the data near the inner edge is due to the fact that the employed masks do not cover the entire width of the OFPC. Near the outer edge, the mask fastener prevented the formation of a sufficiently large unexposed reference surface, thus precluding data analysis in this region.

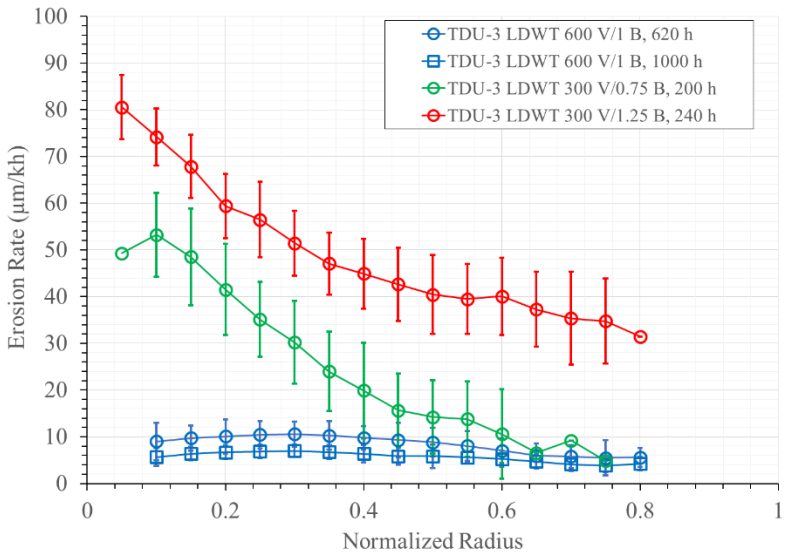

Fig. 10 OFPC erosion rates measured during the TDU-3 LDWT.

As shown in Fig. 10, the OFPC erosion rates largely follow the same trends as those for the IFPC. Specifically, OFPC erosion is observed to increase beyond the measurement uncertainty as the discharge voltage is decreased from 600 V to 300 V and as the magnetic field strength is increased at a fixed discharge voltage of 300 V. Specifically, the erosion rate at 300 V/0.75 B is approximately 4 times higher, on average, at a given radius than for 600 V. Furthermore, the erosion rate is approximately 1.4 times higher, on average, at a given radius for operation at 300 V/1.25 B compared to 300 V/0.75 B. In addition, for all operating conditions, the OFPC erosion is shown to maximize near the discharge channel and then decrease with increasing radius. The observed variations in OFPC erosion with radial position and discharge voltage match results from previous empirical and analytic work, while the observed variation with magnetic field had not previously been investigated [5, 30].

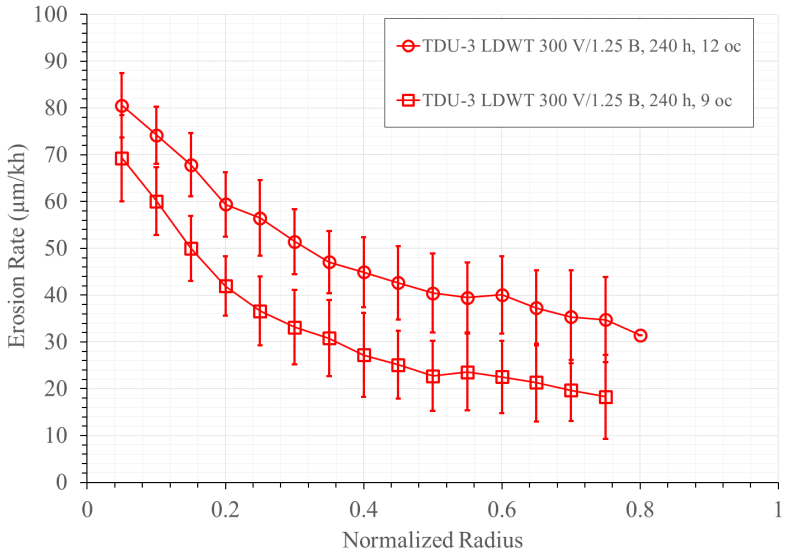

Fig. 11 Comparison of OFPC erosion rates measured near the 12 o'clock (12 oc) and 9 o'clock (9 oc) masks.

Similar to the approach taken with the IFPC, in order to assess the azimuthal symmetry of the OFPC wear mechanisms, profilometry measurements acquired near both the 12 o'clock and 9 o'clock masked regions were compared for the 300 V/1.25 B operating condition. The results are shown as a function of normalized OFPC radius

in Fig. 11. Contrary to the IFPC results, the azimuthal variation in wear rates was greater than the measurement uncertainty, suggesting that the OFPC wear was asymmetric for this operating condition. However, it is important to note that the pre-test surface finish in both of these regions was different. Specifically, the 12 o'clock mask was placed over a region of polished graphite whereas the region near the 9 o'clock mask was unpolished.

Taken together with the observed decrease in IFPC erosion rates over time, this result suggests a possible link between surface finish and erosion rates. Specifically, although polished pre-test, the IFPC has been observed to roughen after plasma exposure. Evidence of this can be seen in Fig. 12(b), which is a post-test image of the pole cover shown in Fig. 12(a) that shows evidence of significant roughening relative to the polished finish achieved pre-test. Once roughened, the results in Fig. 4, suggest that the erosion rates of the IFPC decrease. If true, that would also explain the results in Fig. 11, where the unpolished portion of the OFPC is shown to erode slower than the polished portion. This possibility will be further investigated during the remainder of the LDWT.

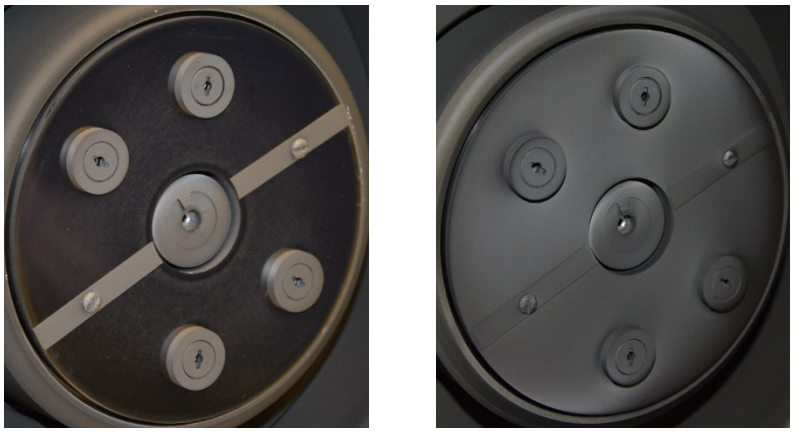

(a) **(b)**

Fig. 12 TDU-3 IFPC (a) before and (b) after completion of a segment of the LDWT.

IV.Conclusion

This work presented a summary and overview of the results acquired during the first four segments (1715 h) of the TDU-3 LDWT. Periodic performance characterizations performed at a set of six fixed reference firing conditions indicated that TDU-3 performance and stability varied by less than the measurement uncertainty throughout the test as well as when compared to results acquired during previous TDU performance and wear characterizations.

Erosion of the inner and outer front pole covers was shown to be a strong function of discharge voltage and magnetic field strength. Specifically, erosion rates at 300 V were shown to be up to four times higher than those at 600 V due to the higher beam divergence at the lower discharge voltage. These rates were also shown to increase with increasing magnetic field strength for operation at 300 V. Consistent with results from previous TDU wear tests, a decrease in IFPC erosion rate was shown with operating time. Observations of lower erosion rates for unpolished sections of the OFPC suggest that this might be caused by the roughening of the pole covers during operation, rather than a change in the near-field plasma properties. Finally, shifting the axial position of the cathode from coplanar to upstream of the IFPC resulted in an 84% reduction in measured erosion rates, thus validating this design approach for mitigating the elevated keeper wear observed during the SDWT.

V.Acknowledgements

The authors would like to thank the Space Technology Mission Directorate through the Solar Electric Propulsion Technology Demonstration Mission Project for funding the joint NASA GRC and JPL development of the HERMeS TDU thrusters and this work. The authors would also like to thank David Jacobson, Tom Haag, and Jon Mackey of GRC and Alejandro Lopez Ortega, Ioannis Mikellides, and James Polk of JPL for all of their work, technical input, and guidance. Finally, the authors would like to thank Taylor Seablom, Chad Joppeck, Kevin Blake, George Jacynycz, Roland Gregg, Josh Gibson, Matt Daugherty, James Szelagowski, James Zakany, and all of the engineers and technicians of the Space Environments Test Branch (FTF0) for the fabrication, assembly of the test setup, and operation of the vacuum facility.

VI. References

[1] Congress, "National Aeronautics and Space Administration Transition Authorizatin Act of 2017," 2017.

[2] Gerstenmaier, W., "Progress in Defining the Deep Space Gateway and Transport Plan," *NASA Advisory Council Human Exploration and Operations Committee Meeting*, Washington, DC, 2017.

[3] Smith, B. K., Nazario, M. L., and Cunningham, C. C., "Solar Electric Propulsion Vehicle Demonstration to Support Future Space Exploration Missions", *Space Propulsion 2012*, Bordeaux France, 2012.

[4] Williams, G., Gilland, J. H., Peterson, P. Y., Kamhawi, H., Huang, W., Swiatek, M., Joppeck, C., Yim, J., and Haag, T. W., "2000-hour Wear-Testing of the HERMeS Thruster," *52nd AIAA/SAE/ASEE Joint Propulsion Conference*, AIAA Paper 2016-5025, 2016.

[5] Williams, G. J., Kamhawi, H., Choi, M., Haag, T., Huang, W., Herman, D. A., Gilland, J. H., and Peterson, P. Y., "Wear Trends of the HERMeS Thruster as a Function of Throttle Point," *35th International Electric Propulsion Conference*, IEPC Paper 2017-207, Electric Rocket Propulsion Society, Fairview Park, OH, 2017.

[6] Hofer, R., Polk, J., Sekerak, M., Mikellides, I., Kamhawi, H., Verhey, T., Herman, D., Williams,G., "The 12.5 kW Hall Effect Rocket with Magnetic Shielding (HERMeS) for the Asteroid Redirect Robotic Mission," *52nd AIAA/SAE/ASEE Joint Propulsion Conference*, AIAA paper 2016-4825, 2016.

[7] Kamhawi, H., Huang, W., Gilland, J., Haag, T., Mackey, J., Yim, J., Pinero, L, Williams, G., Peterson, P., Herman, D. , "Performance, Stability, and Plume Characterization of the HERMeS Thruster with Boron Nitride Silica Composite Discharge Channel," *35th International Electric Propulsion Conference*, IEPC Paper 2017-392, Eelectric Rocket Propulsion Society, Fairview Park, OH, 2017.

[8] Mikellides, I.G., Katz, I., Hofer, R.R., Goebel, D.M, de Grys, K., and Mathers, A., "Magnetic shielding of the channel walls in a Hall plasma accelerator," *Physics of Plasmas*, Vol. 18, No. 3, 2011, pp. 033501.

[9] Mikellides, I.G., Katz, I., Hofer, R.R., and Goebel, D.M,, "Magnetic shielding of a laboratory Hall thruster. I. Theory and validation," *Journal of Applied Physics*, Vol. 115, No. 4, 2014, pp. 043303.

[10] Mikellides, I.G., Katz, I., Hofer, R.R., Goebel, D.M, de Grys, K., and Mathers, A., "magnetic Shielding of the Acceleration Channel Walls in a Long-Life Hall Thruster," *46th AIAA/ASME/SAE Joint Porpulsion Conference & Exhibit*, AIAA Paper 2010-6942, 2010.

[11] Snyder, J., Baldwin, J., Frieman, J. D., Walker, M. L. R., Hicks, N. S., Polzin, K. A., and Singleton, J. T., "Recommended Practice for Flow Control and Measurement in Electric Propulsion Testing," *Journal of Propulsion and Power*, Vol. 33, No. 3, 2017, pp. 556-565.

[12] Piñero, L.R., "The Impact of Harness Impedance on Hall Thruster Discharge Oscillations," *35th International Electric Propulsion Conference*, IEPC Paper 2017-023, Electric Rocket Propulsion Society, Fairview Park, OH, 2017.

[13] Huang, W., Kamhawi, H., Haag, T.W., Lopez Ortega, A., and Mikellides, I.G., "Facility Effect Characterization Test of NASA's HERMeS Hall Thruster," *52nd AIAA/SAE/ASEE Joint Propulsion Conference*, AIAA Paper 2016-4828, 2016.

[14] Kamhawi, H., Huang, W., Haag, T.W., Yim, J.T., Herman, D.A., Peterson, P.Y., Williams, G., Gilland, J., Hofer, R., and Mikellides, I.G., "Performance, Facility Pressure Effects, and Stability Characterization Tests of NASA's Hall Effect Rocket with Magnetic Shielding Thruster," *52nd AIAA/SAE/ASEE Joint Propulsion Conference*, AIAA Paper 2016-4826, 2016.

[15] Peterson, P.Y., Kamhawi, H., Huang, W., Yim, J.T., Herman, D.A., Williams, G., Gilland, J., and Hofer, R., "NASA's HERMeS Hall Thruster Electrical Configuration Characterization," *52nd AIAA/SAE/ASEE Joint Propulsion Conference*, AIAA Paper 2016-5027, 2016.

[16] Frieman, J.D., King, S.T., Walker, M.L.R., Khayms, V., and King, D., "Role of a Conducting Vacuum Chamber in the Hall Effect Thruster Electrical Circuit," *Journal of Propulsion and Power*, Vol. 30, No. 6, pp. 1471–1479, 2014.

[17] Lobo, M.J., "Electric Propulsion Laboratory," NASA Glenn Research Center, URL: https://www1.grc.nasa.gov/facilities/epl/ [retrieved 20 December 2017].

[18] Yim, J.T., Herman, D.A, and Burt, J.M., "Modeling Analysis for NASA GRC Vacuum Facility 5 Upgrade," NASA TM-2013-216496, 2013.

[19] Yim, J.T. and Burt, J.M., "Characterization of Vacuum Facility Background Gas Through Simulation and Considerations for Electric Propulsion Ground Testing," *51st AIAA/SAE/ASEE Joint Propulsion Conference*, AIAA Paper 2015-3825, 2015.

[20] Dankanich, J.W., Walker, M., Swiatek, M.W., and Yim, J.T., "Recommended Practice for Pressure Measurement and Calculation of Effective Pumping Speed in Electric Propulsion Testing," *Journal of Propulsion and Power*, Vol. 33, No. 3, 2017, pp. 668-680.

[21] "Standard Practice for Ionization Gage Application to Space Simulators," ASTM E296-70, 2015.
[22] Gilland, J. H., Williams, G., Burt, J. M., and Yim, J., "Carbon Back Sputter Modeling for Hall Thruster Testing," *52nd AIAA/SAE/ASEE Joint Propulsion Conference*, AIAA Paper 2016-4941, 2016.
[23] Huang, W., Kamhawi, H., and Haag, T.W., "Plasma Oscillation Characterization of NASA's HERMeS Hall Thruster via High Speed Imaging," 52nd AIAA/SAE/ASEE Joint Propulsion Conference, AIAA 2016-4829, 2016.
[24] Xu, K.G., and Walker, M.L.R., "High-power, null-type, inverted pendulum thrust stand," *Review of Scientific Instructiments*, Vol. 80, No. 5, 2009, pp. 055103.
[25] Polk, J.E., Pancotti, A., Haag, T., King, S., Walker, M.L.R., Blakel, J., and Ziemer, J., "Recommended Practices in Thrust Measurements," *33rd International Electric Propulsion Conference*, IEPC Paper 2013-440, Electric Rocket Propulsion Society, Fairview Park, OH, 2013.
[26] Haag, T.W., "Thrust stand for high-power electric propulsion devices," *Review of Scientific Instructiments*, Vol. 62, No. 5, 1991, pp. 1186–1191.
[27] Mackey, J., Haag, T. W., Peterson, P. Y., and Kamhawi, H., "Uncertainty in Inverted Pendulum Thrust Measurements," *54th AIAA/SAE/ASEE Joint Propulsion Conference*, 2018.
[28] I. O. f. Standardization, "ISO 5436-1:2000 Geometrical Product Specifications (GPS) - Surface texture: Profile method; Measurement standards - Part 1: Material measures," ed, 2003.
[29] Fisher, J., Wilson, A., King, D., Meyer, S., de Grys, K., and Werthman, L., "The Development and Qualification of a 4.5 kW Hall Thruster Propulsion Subsystem," *39th AIAAASMESAEASEE Joint Propulsion Conference and Exhibit,* AIAA Paper 2003-4551, 2003.
[30] Lopez Ortega, A., Mikellides, I.G., and Chaplin, V.H., "Numerical Simulations for the Assessment of Erosion in the 12.5-kW Hall Effect Rocket with Magnetic Shielding (HERMeS)," *35th International Electric Propulsion Conference*, IEPC Paper 2017-154, Electric Rocket Propulsion Society, Fairview Park, OH, 2017
[31] Polk, J. E., Lobbia, R., Barriault, A., Guerrero, P., Mikellides, I., and Lopez Ortega, A., "Inner Front Pole Cover Erosion in the 12.5 kW HERMeS Hall Thruster Over a Range of Operating Conditions," 35th International Electric Propulsion Conference, IEPC Paper 2017-409, Eelectric Rocket Propulsion Society, Fairview Park, OH, 2017.
[32] Chaplin, V. H., Conversano, R. W., Lobbia, R. B., Lopez Ortega, A., Mikellides, I. G., Hofer, R. R., and Jorns, B. A., "Laser-Induced Fluorescence Measurements of the Acceleration Zone in the 12.5 kW HERMeS Hall Thruster," *35th International Electric Propulsion Conference*, IEPC Paper 2017-229, Electric Rocket Propulsion Society, Fairview Park, OH, 2017.
[33] Lopez Ortega, A., Mikellides, I.G., and Goebel, D.M., "Numerical Simulations for Life Assessments of the BaO and LaB 6 Cathode Options in the Hall Effect Rocket with Magnetic Shielding (HERMeS)," *35th International Electric Propulsion Conference*, IEPC Paper 2017-152, Electric Rocket Propulsion Society, Fairview Park, OH, 2017.